NRL Report 7645

Surface and Bottom Magnetic Survey in the Area of the Bermuda Rise

P. B. ALERS, J. M. BERGIN, AND D. GREENEWALT

Ocean Sciences Division

December 21, 1973

NAVAL RESEARCH LABORATORY
Washington, D.C.

REPORT DOCUMENTATION PAGE		READ INSTRUCTIONS BEFORE COMPLETING FORM
1. REPORT NUMBER NRL Report 7645	2. GOVT ACCESSION NO.	3. RECIPIENT'S CATALOG NUMBER
4. TITLE *(and Subtitle)* SURFACE AND BOTTOM MAGNETIC SURVEY IN THE AREA OF THE BERMUDA RISE		5. TYPE OF REPORT & PERIOD COVERED Summary of a continuing problem. 6. PERFORMING ORG. REPORT NUMBER
7. AUTHOR*(s)* P. B. Alers, J. M. Bergin, and D. Greenewalt		8. CONTRACT OR GRANT NUMBER*(s)*
9. PERFORMING ORGANIZATION NAME AND ADDRESS Naval Research Laboratory Washington, D.C. 20375		10. PROGRAM ELEMENT, PROJECT, TASK AREA & WORK UNIT NUMBERS NRL Problem G03-01 RR 131-03-41-5905
11. CONTROLLING OFFICE NAME AND ADDRESS Department of the Navy Office of Naval Research Washington, D.C. 20361		12. REPORT DATE December 21, 1973 13. NUMBER OF PAGES 36
14. MONITORING AGENCY NAME & ADDRESS*(if different from Controlling Office)*		15. SECURITY CLASS. *(of this report)* Unclassified 15a. DECLASSIFICATION/DOWNGRADING SCHEDULE
16. DISTRIBUTION STATEMENT *(of this Report)* Approved for public release; distribution unlimited.		
17. DISTRIBUTION STATEMENT *(of the abstract entered in Block 20, if different from Report)*		
18. SUPPLEMENTARY NOTES		
19. KEY WORDS *(Continue on reverse side if necessary and identify by block number)* Geomagnetism, Bermuda Rise Sea floor Magnetometer Upward continuation Magnetic noise		

20. ABSTRACT *(Continue on reverse side if necessary and identify by block number)*

A shipborne investigation of sea-floor magnetism was carried out in the three Marsden squares immediately west of Bermuda in November 1972. Both deep and surface magnetometers were used. The deep record was examined for the presence of short-wavelength (<5 km) geological anomalies; none were found. The bottom record was mathematically scaled to the surface and was found to be consistent with the surface record. The surface data were filtered to separate various noise components, and wave noise, geomagnetic noise, and geological noise sources were all identified. The

20. (Continued)

upward continuation results, a magnetic chart of the area, and field data along representative tracks, together with spectra of peak height vs wavelength, were all derived. A detailed discussion of two different filter techniques is included as an appendix.

CONTENTS

SURFACE AND BOTTOM MAGNETIC SURVEY IN THE AREA OF THE BERMUDA RISE

INTRODUCTION

The Navy, as part of its antisubmarine warfare effort, has long been engaged in making magnetic field measurements at sea. Because of the high sensitivity of the instruments in use, the nature of environmental background noise has been particularly important. There are three major categories of noninstrumental interference which are of current concern: (a) ocean wave noise, (b) ionospheric or geomagnetic noise, and (c) geological noise. Both wave and geomagnetic noise are genuinely time dependent, but geological noise, caused by features fixed in the sea floor, depends on the speed of the detector. The periods for wave noise fall in the range of 10 s or less; short period waves are generally of low amplitude and their magnetic contribution is small, but low-amplitude, long-period waves produce signals which appear in our records as an increase in background noise. Geomagnetic noise, except for diurnal variations, has periods of the order of a few minutes. Geological noise arising from bottom features ranging from 1 km to, say, 100 km in width, is well separated in time from other noise sources when measured from a ship, but it falls squarely in the 10-1000 s range when observed from a 200 knot aircraft. It is therefore indistinguishable from geomagnetic noise in the airborne case, and both tend to interfere with submarine signatures. The use of gradiometer techniques can minimize the effects of geomagnetic noise, but geological noise is not so easily removed. It is desirable to identify those areas of the ocean where sea-floor geology interferes with efficient magnetic detection so that other techniques might be used. To make such an identification, magnetic records are taken from ship-towed instruments in selected areas to allow us to study geological noise without the masking effects of geomagnetic noise. The measurements are made by towing a sensor close to the sea floor and another at the surface. The bottom record shows geological features quite clearly, with geomagnetic noise appearing only as a perturbation. In the surface record, the two appear with comparable magnitudes but different periods. The bottom record is mathematically scaled to the surface (upward continuation), and thus the geological component in the surface record can be identified and separated.

This report deals with one such survey carried out in the waters adjacent to Bermuda. Both magnetometers used were of the resonance type, and the sampling rate was normally 10 s. This served to cut out noise arising from wave action in light to moderate seas, and we were able to gather a great deal of information on the distribution and extent of the sea-floor anomalies.

EQUIPMENT

The deep magnetometer was one of NRL design, towed at a depth of 4000 to 5000 m. The surface instrument was a commercial marine magnetometer (Geometrics Model G-801) towed about 300 m aft of the ship, the USNS MIZAR (T-AGOR-11). A 43-digit data acquisition system was used to record on 7-track magnetic tape the fields read by both

Manuscript submitted August 16, 1973.

magnetometers as well as the outputs of a 24-hr clock, a fiducial counter, and the settings of a series of numerical thumbwheel switches on which were entered the Julian day, latitude, longitude, and water depth. As noted above, all inputs were recorded every 10 s, with the switch readings reset at half-hour intervals. In addition to the tape recording system, two strip-chart recorders presented the magnetometer outputs in real time. This not only provided us with a visible record as the data were being gathered, but also furnished a backup system in case the digital equipment failed to function properly.

SURVEY TRACK AND PRELIMINARY OBSERVATIONS

The surface magnetometer was deployed during the trip to the operations area, and its output shows clearly the differences between the magnetic quiet zone which lies off the North American continental shelf and the more active area in the vicinity of Bermuda. Figure 1 shows the magnetic record from 34°53'N, 72°38'W, to 32°31'N, 66°10'W, a distance of about 650 km. The transition from "quiet" to "noisy" can be seen to be fairly abrupt, with the magnetic variations in the noisy area running 100-300 γ in peak-to-peak amplitude and 8-12 km in width. The steady downward trend in the background field is part of the worldwide variation of the earth's field.

The operating area itself consisted of a rectangle composed of the three Marsden squares bounded by 33°N, 65°W, 32°N, and 68°W, lying immediately west of Bermuda. The tracks followed are shown in Fig. 2. The deep magnetometer was not deployed at all times; the tracks where both it and the surface magnetometer were used are shown as solid lines, and where the surface instrument alone was used the lines are dotted. The square closest to Bermuda contains the highest density of tracks because we felt that small-scale anomalies would most likely occur close to the island.

DATA TREATMENT

The main body of bottom data, which consisted of digital magnetic field readings recorded as a function of time, was first converted to field vs distance with the necessary corrections and smoothing and then incorporated into an upward continuation program and compared with surface data taken at the same time. The results of these calculations are discussed in the first part of the next section.

The surface data were treated in two ways. A magnetic chart of the area was constructed to provide an overall view of the fixed magnetic features detectable at the surface. This is presented after the deep data section. Then, since the presence of anomalies less than 10 km in width was of special interest, Fourier analysis was used on several magnetic records to reveal the presence of any such structures. Eight such magnetograms and their spectra are described and presented.

In Appendix A a discussion of two different methods of filtering the data, with examples, is presented. Such a process is necessary to identify features in a particular wavelength band. Further, with such information at hand, such sorting procedures as counting the number of features of a certain wavelength or amplitude in a given record can be carried out.

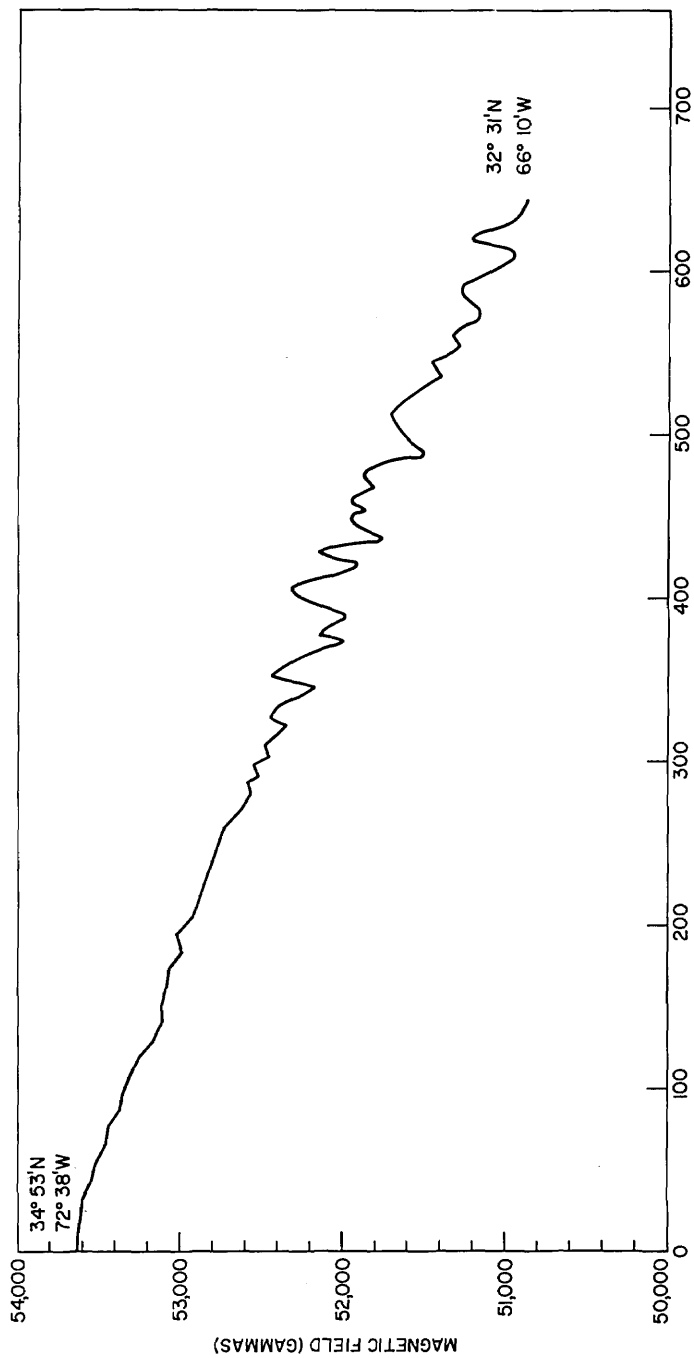

Fig. 1 — Surface magnetic record taken during transit to operating area between points shown. Contrast between quiet zone and magnetically active area is apparent.

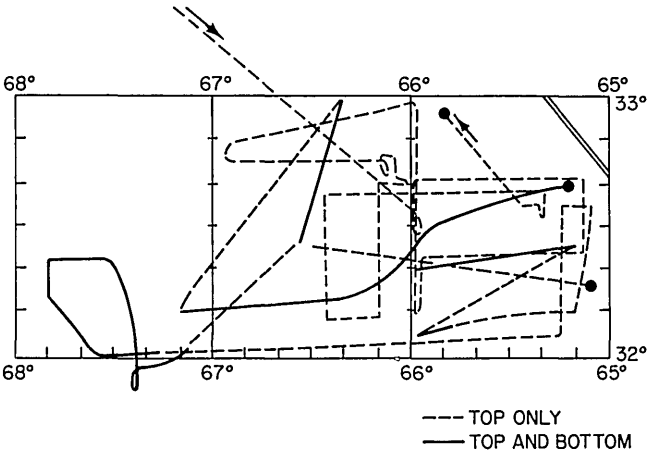

Fig. 2 — Tracks followed in operating area. Surface and bottom data were taken along solid tracks; surface data only were gathered on dotted tracks.

RESULTS AND CONCLUSIONS

Deep Data

The magnetic field close to the ocean bottom was measured along the tracks shown in Fig. 2. The depth of the deep magnetometer was determined by the use of a pinger (Benthos Model 2213) clamped to the towing wire 100 ft above the magnetometer. The magnetometer was towed at a fairly constant depth of 4 km below the surface, or about 1 km above the bottom for this area. It lagged the ship by about 2 km at the towing speed used. Precision of measurement, estimated from the variation of the individual magnetic field measurements, was generally better than $\pm 5\ \gamma$. The surface magnetometer was in operation throughout the deep magnetometer measurements.

Figure 3 shows a set of near-bottom data together with the corresponding surface data. The deep-field oscillations are considerably larger in amplitude, but the wavelengths present are roughly the same. In order to estimate the detection limits of the deep system we can assume that about 1/2 km of sediment overlies the bottom basalts in this area. This means that the deep magnetometer was being towed about 1.5 km above the magnetic basement. If we combine the detection sensitivity given above with the maximum likely amplitude of a sinusoidal bottom anomaly, 1000γ, we can calculate from potential theory that such an anomaly would be detectable at 1.5 km only if it were more than 1.8 km in wavelength. For a more realistic amplitude of 500γ, the wavelength necessary for detection increases to 2.1 km. The traces in Figure 3 indicate no features smaller than about 10 km, excluding those attributable to changes in course or speed.

The same analysis can be applied to fields detectable at the surface, 5.5 km above the magnetic sources in these waters. A sinusoidal anomaly of 1000γ and 4 km wavelength gives a surface field of 0.17γ; a similar 1 km anomaly is undetectable. The geological magnetic noise measured at the surface in this area can therefore be considered quite negligible in the 1-4 km wavelength range.

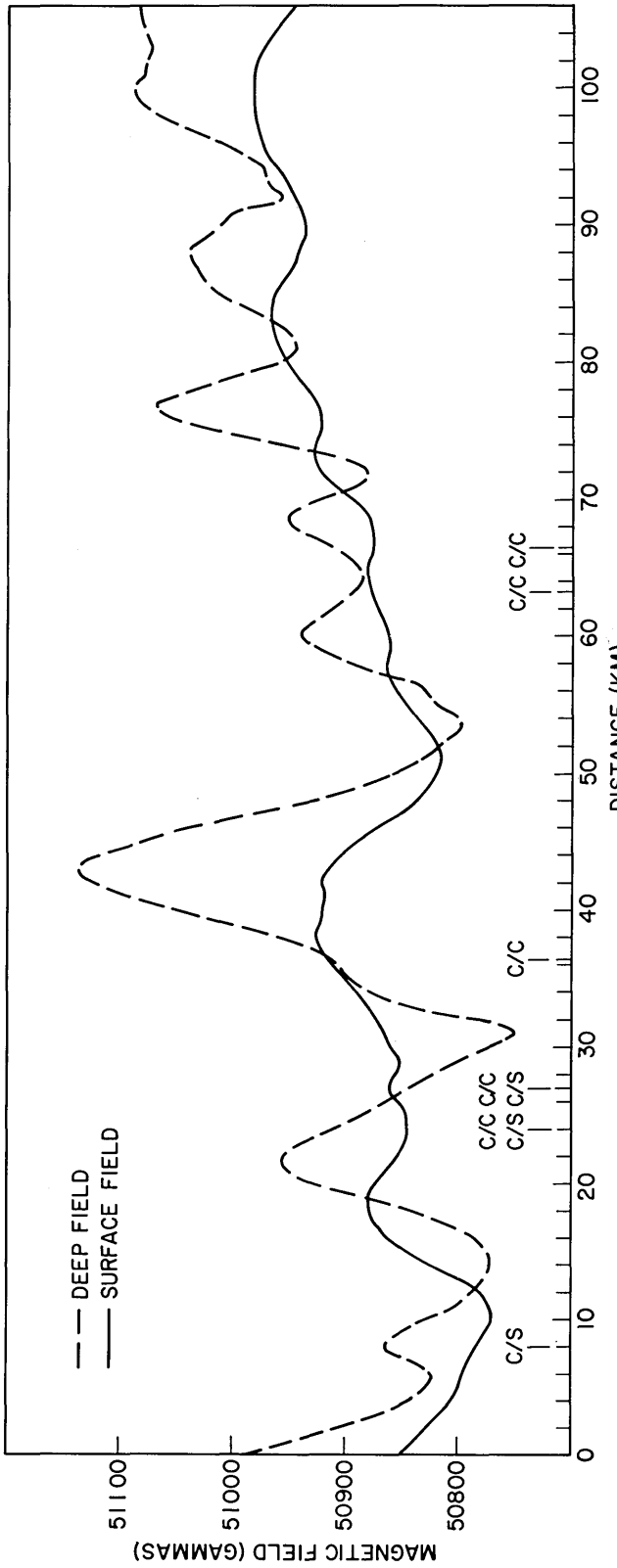

Fig. 3 — Deep magnetic record (dotted) compared to surface record (solid). Features in the two patterns are displaced by about 2 km because of the difference in horizontal position of the two transducers.

Figure 4 shows the deep magnetic field continued upward by the method of Henderson and Zietz* if we assume a two-dimensional field. Data points were shifted forward (right) 2 km to account for the lag of the deep magnetometer relative to the ship and surface magnetometer, and the field has been reduced in absolute value by 100γ (the dipole gradient here is about 25 γ/km) for comparison with the surface field. The agreement between the fields is generally good, considering the not necessarily correct assumption that the field sources are two dimensional. Differences between the upward continued deep field and the surface field may in part be due to time changes in the earth's field, which are not only altered by the layer of seawater between magnetometers, but are also reduced by the process of upward continuation where they appear in the deep field. Most of the differences between the fields shown in Fig. 4 are probably due to course and speed changes, which appear to cause variations in the surface field. Some of these changes are marked in the figure. The difficulties involved in studying short-wavelength variations by means of surface measurement alone should be fairly clear. Significant variations at the surface may be as low as a few hundredths of a gamma, a value below the sensitivity of most instruments. The noise, however, which may be due to ship maneuvers or temporal variation of the field, is three orders of magnitude larger than the signal of interest. If short-wavelength spatial anomalies are to be investigated, it is necessary to measure them close to their origin.

Magnetic Chart

To summarize all of the surface magnetic data taken in the Bermuda area, a magnetic chart was prepared to show magnetic structure as a function of position (Fig. 5). To accomplish this, the navigation data taken at half-hour intervals throughout the trip were combined with the magnetic field strengths recorded on the analog record. In locations where the field changed rapidly, readings were taken more frequently and the positions interpolated.

Navigational fixes were made by use of Loran-C and the satellite navigation system. The fixes used for the chart were, in general, Loran fixes; satellite information was used to correct the Loran data from time to time during the trip. The discrepancies between the two fixes were rarely more than 1.5 mi and were usually smaller.

The fields as plotted are the so-called residual fields, that is, the observed field minus the earth's background field as calculated from the 1965 International Geomagnetic Reference Field (IGRF). The diurnal correction was introduced somewhat more empirically. The earth's magnetic field exhibits a diurnal variation because of charged particles from the sun entering the ionosphere. The maximum variation takes place at local noon at any given point on the earth's surface, and the total perturbation lasts about 4 hr. We were able to construct a chart of diurnal variations for each day from a partial record obtained from a land-based magnetometer we placed ashore in Bermuda and from the magnetograms recorded by observatories in Puerto Rico and Fredericksburg, Va.† The amplitude of these variations on otherwise quiet days amounted to about -50 γ, and the records used to produce the chart were corrected accordingly. The overall effect was comparatively small.

*R.G. Henderson and I. Zeitz, Geophys. 14, 517 (1949).

†The magnetograms from the Fredericksburg, Virginia and the San Juan Magnetic Observatory were provided by the Magnetics Division, Naval Oceanographic Office, and through them from the Environmental Data Service, National Oceanographic and Atmospheric Administration, Boulder, Colorado.

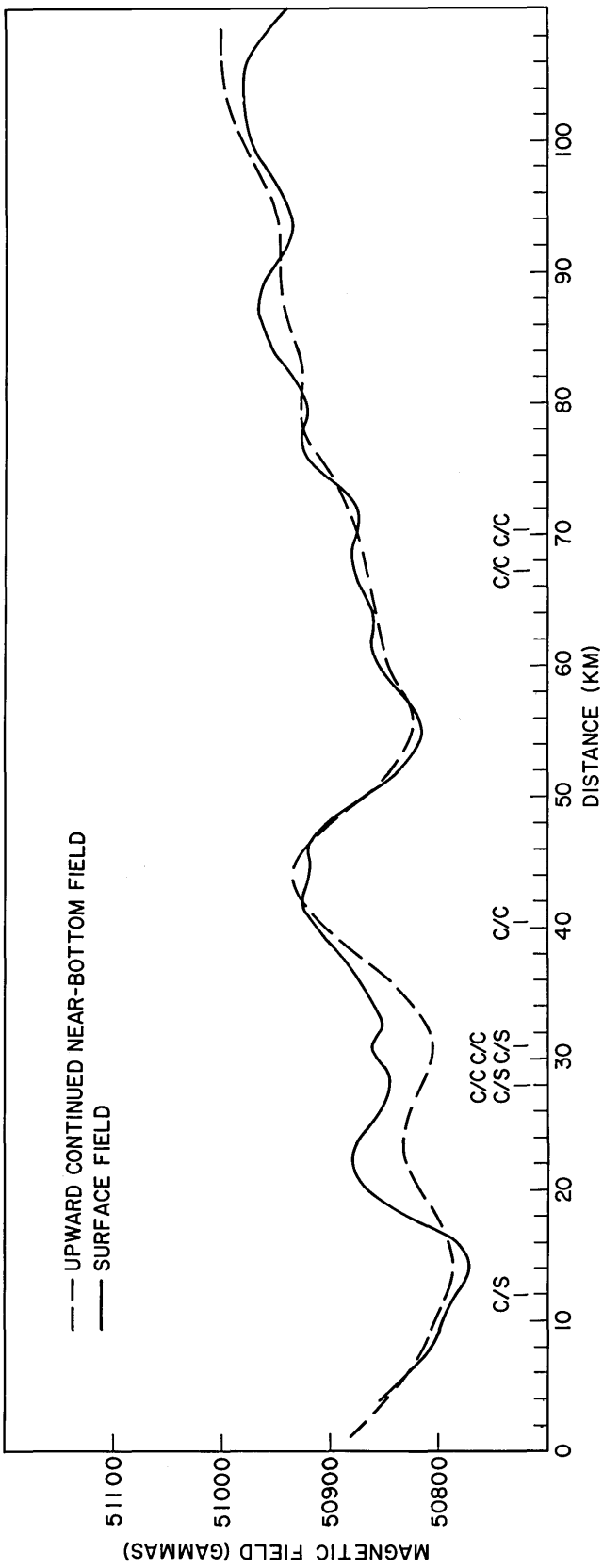

Fig. 4 — The results of continuation of the bottom record up to the surface. Small variations can be attributed to course (c/c) or course and speed (c/s) changes which took place during the track and are noted on the distance axis.

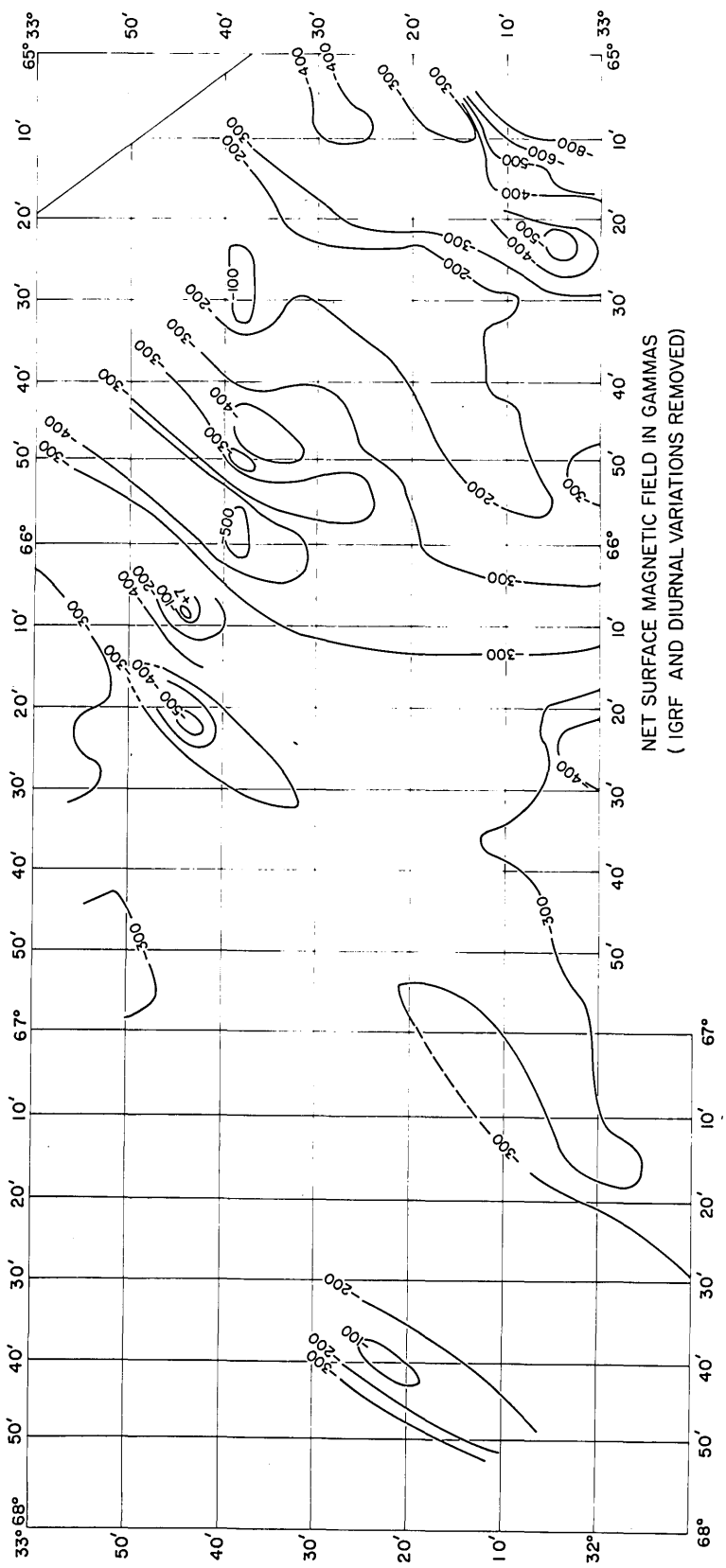

Fig. 5 — Magnetic chart derived from surface readings and navigation data. The fields shown are those obtained by subtracting the International Geomagnetic Reference Field (IGRF) from the observed fields.

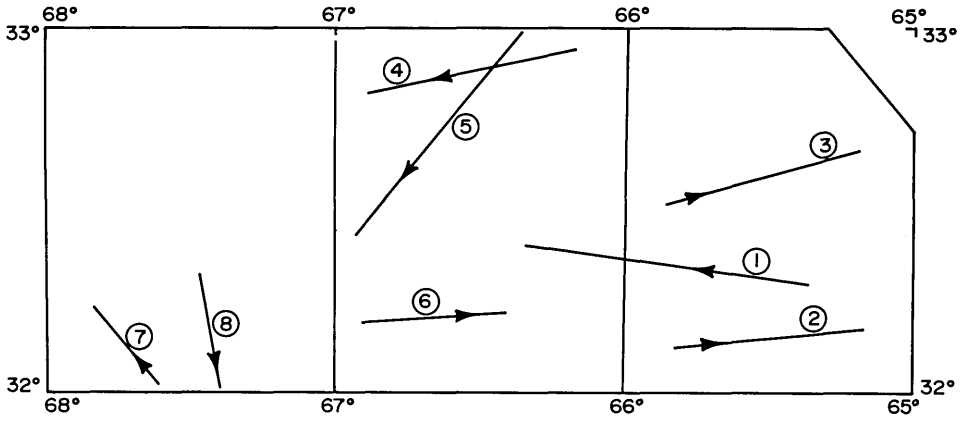

Fig. 6 — Tracks selected to show typical surface magnetograms in the area

The main magnetic feature in the entire area is associated with a small seamount located at 32°44′N, 66°08′W. The peak (residual) field reading at this point is +7γ, the only positive reading recorded. The rest of the area runs some 200-500γ below the IGRF. An additional feature is the line of anomalies running WNW from about 65°40′ to 66°30′, a system which includes the seamount. Data are not extensive enough to identify this with a larger fracture zone, but the configuration is suggestive. A strong negative trend is apparent in the southeastern corner of the area, but the bottom rises rapidly near the banks southwest of Bermuda itself, so such behavior is not surprising.

Sample Magnetograms

Figures 7-14 present typical surface data gathered on tracks distributed throughout the area. Each one represents a straight track located as shown in Fig. 6. The fields are residual, obtained by subtracting the IGRF from the fields actually measured. In addition we present the results of the Fourier analysis of each magnetogram in order to show the amplitude distribution of the anomalies as a function of wavelength. It appears that the strongest anomalies have the longest wavelengths. This is because such anomalies present a uniform field to the detector over a distance that is long compared to the detector-sea-floor distance. Short-wavelength anomalies, on the other hand, are due to successive stripes magnetized in opposite directions, and when the width of each stripe is comparable to the water depth, the resultant field seen by a surface detector is greatly diminished. It is for this reason that deep-tow magnetic data are important in determining the level of short-wave geological noise to be expected in the deep ocean.

Since the water depth in this area is of the order of 5 km except near Bermuda itself, the surface magnetic peaks observed below this wavelength should not be considered as due to geological sources; the bottom record indicates this clearly. The signals at the lower wavelengths are actually dependent on time rather than distance and on each field-vs-wavelength curve a distance-time equivalence figure is given, as determined by the ship's speed on that track. Track 4, for example, was run in heavy seas, and the noise level for that track is correspondingly high; high-speed runs, as in Track 5, also tend to increase background noise. On the other hand, Tracks 6, 7, and 8 show peaks around 1 km as well as a higher level of noise in the 1- to 10-km range which we attribute to sideways motions of the ship. Its speed, 1 knot, was so low that it periodically lost steerageway.

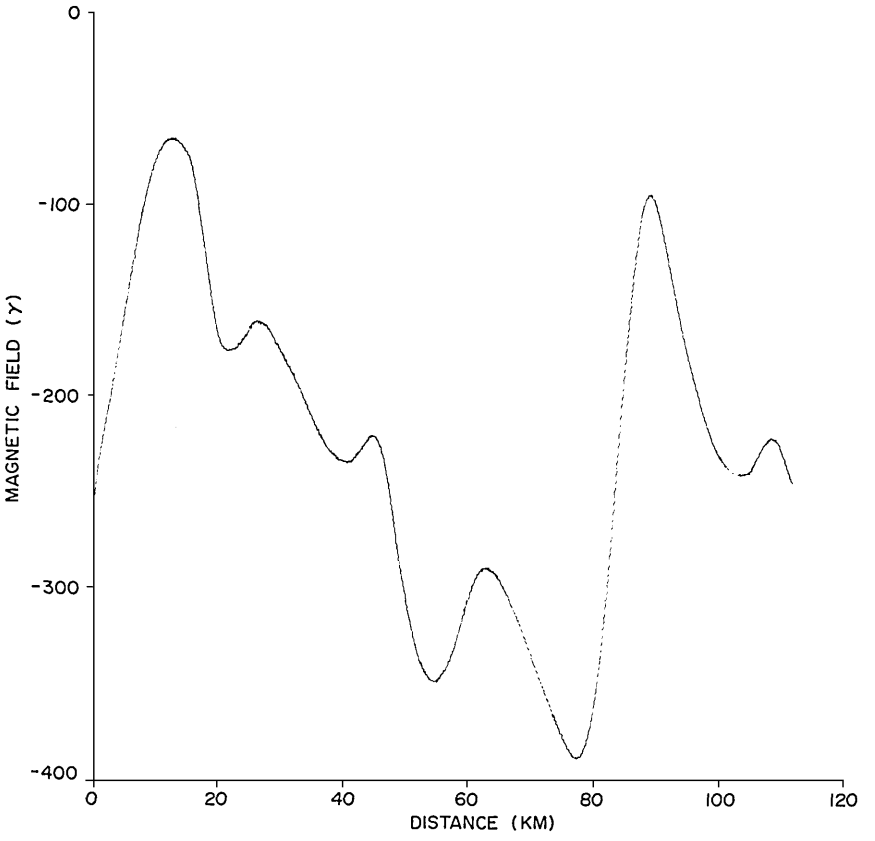

Fig. 7a — Residual field vs distance for Track 1

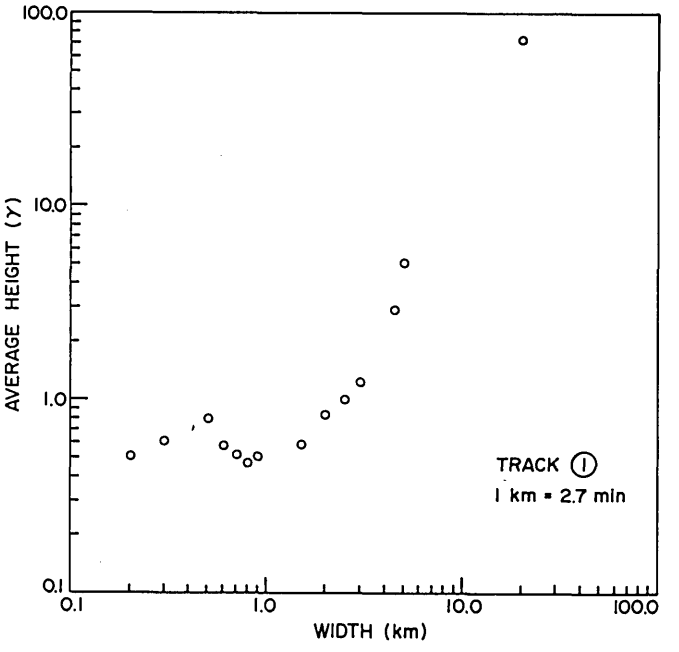

Fig. 7b — Spectrum of average peak heights vs corresponding wavelengths for Track 1

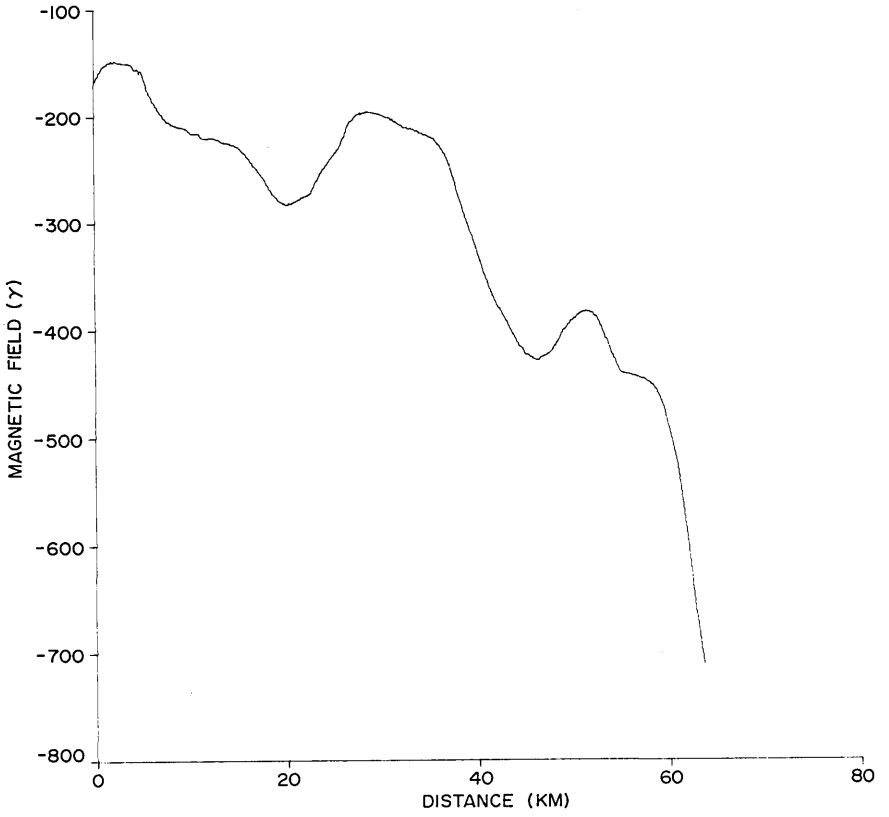

Fig. 8a — Residual field vs distance for Track 2

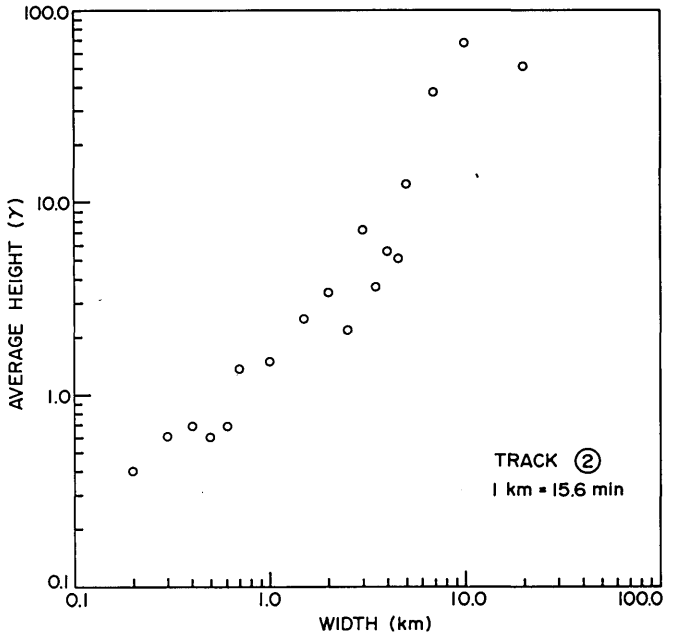

Fig. 8b — Spectrum of average peak heights vs corresponding wavelengths for Track 2

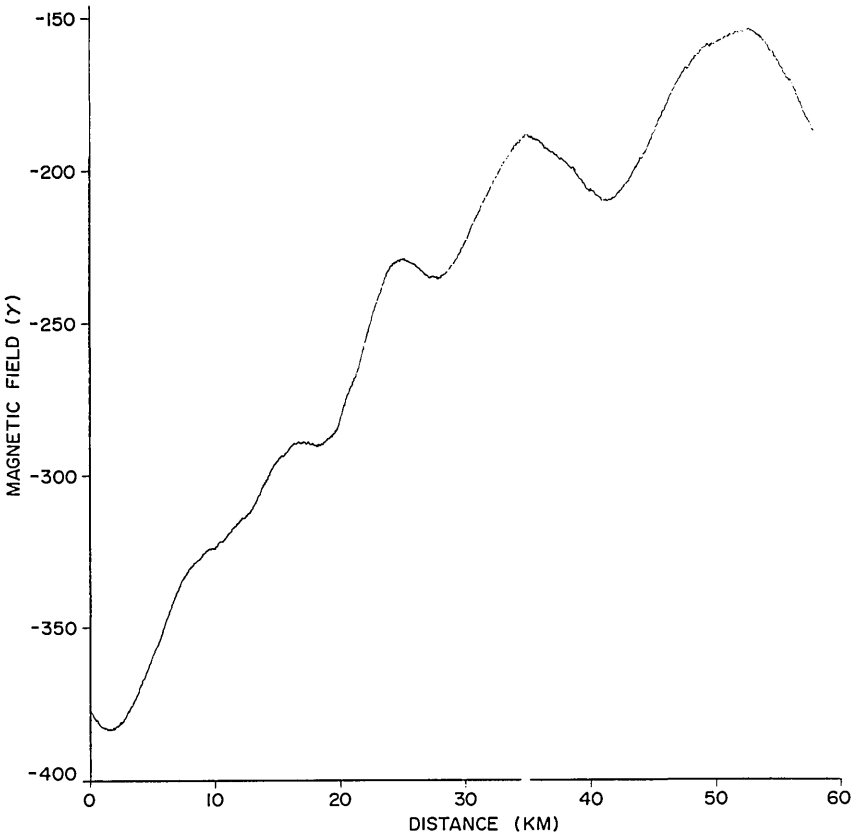

Fig. 9a — Residual field vs distance for Track 3

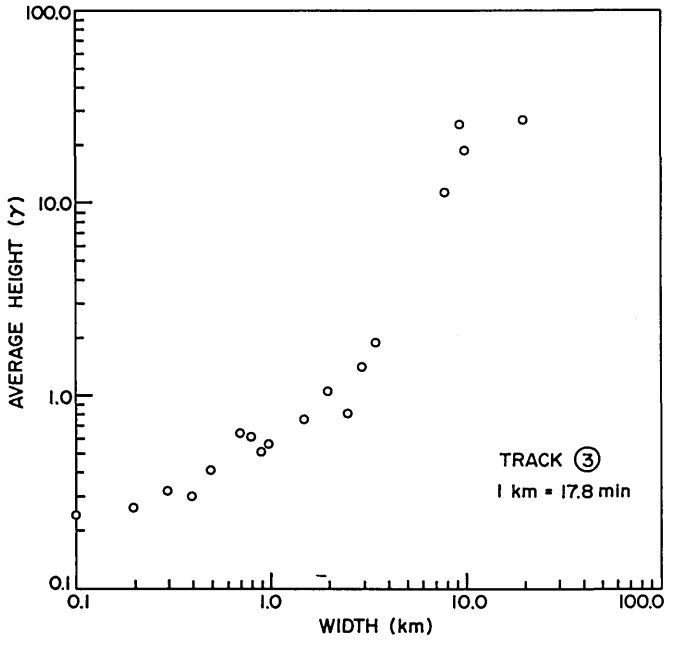

Fig. 9b — Spectrum of average peak heights vs corresponding wavelengths for Track 3

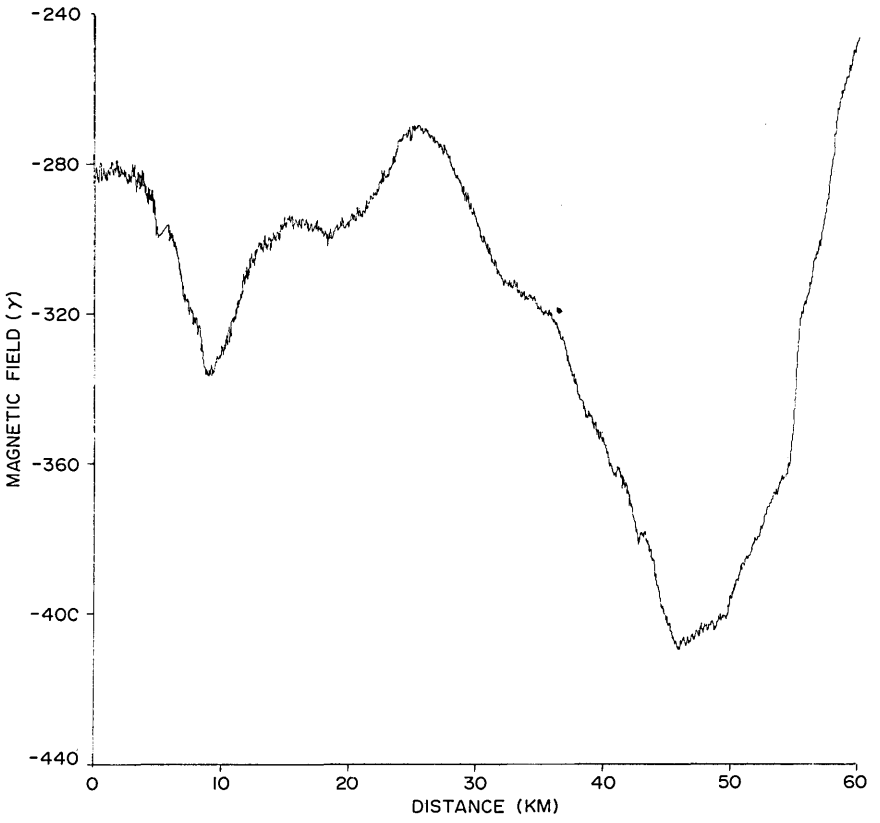

Fig. 10a — Residual field vs distance for Track 4

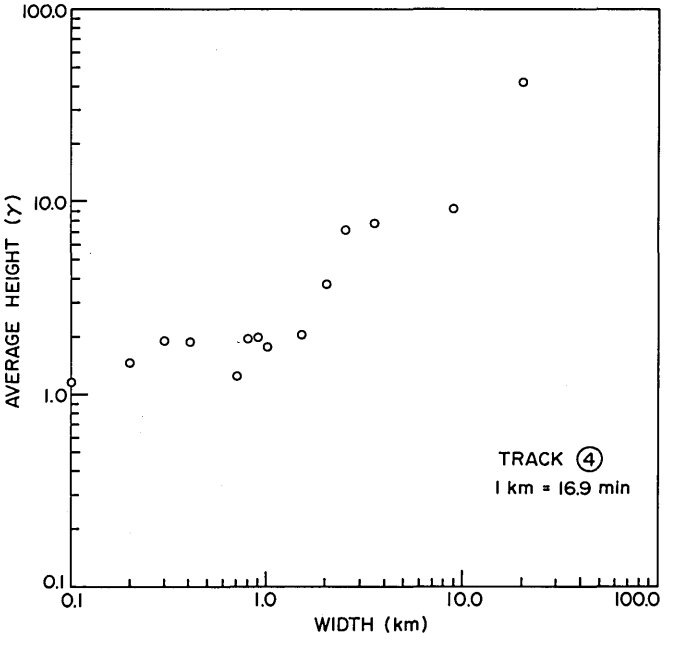

Fig. 10b — Spectrum of average peak heights vs corresponding wavelengths for Track 4

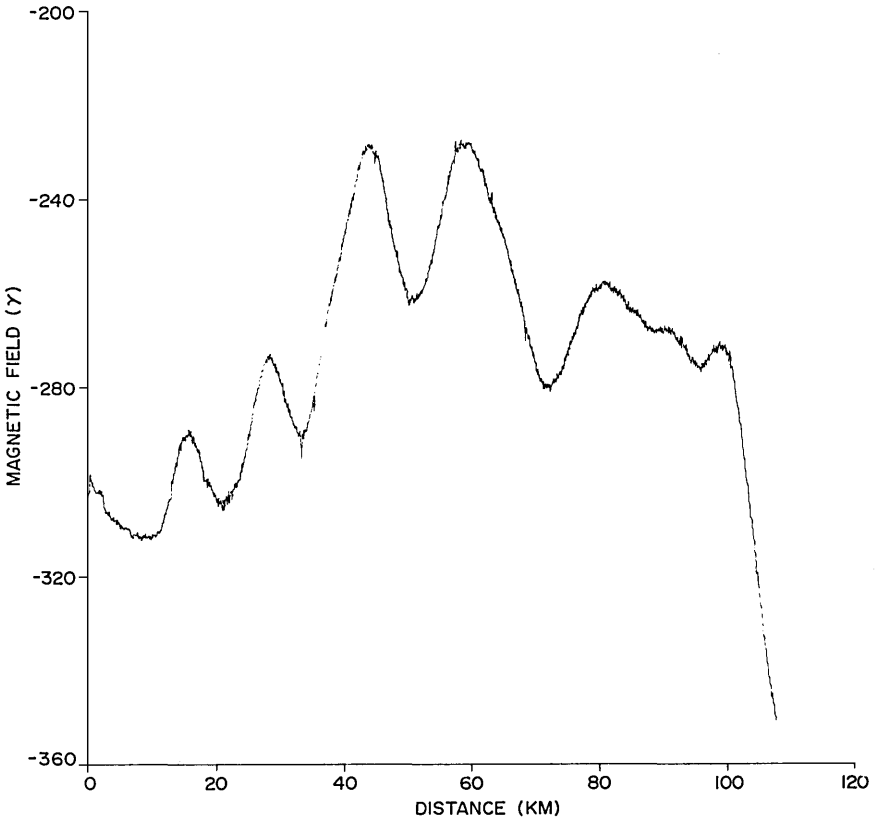

Fig. 11a — Residual field vs distance for Track 5

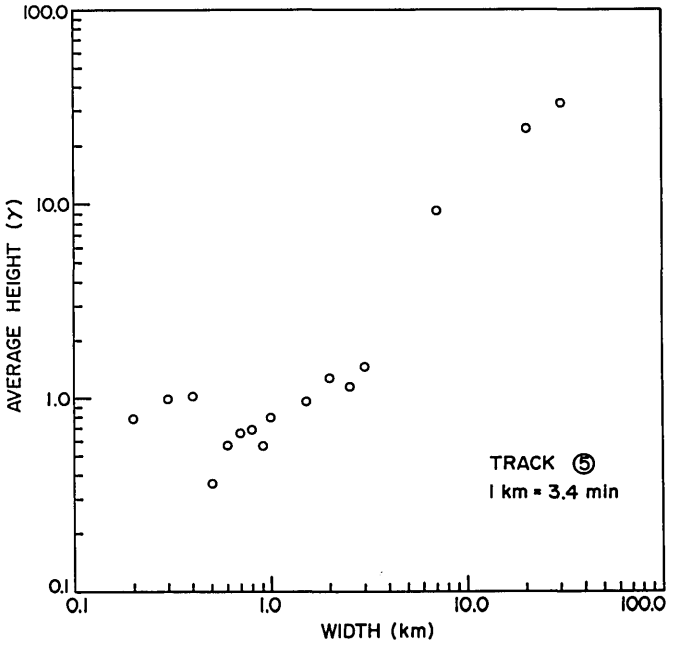

Fig. 11b — Spectrum of average peak heights vs corresponding wavelengths for Track 5

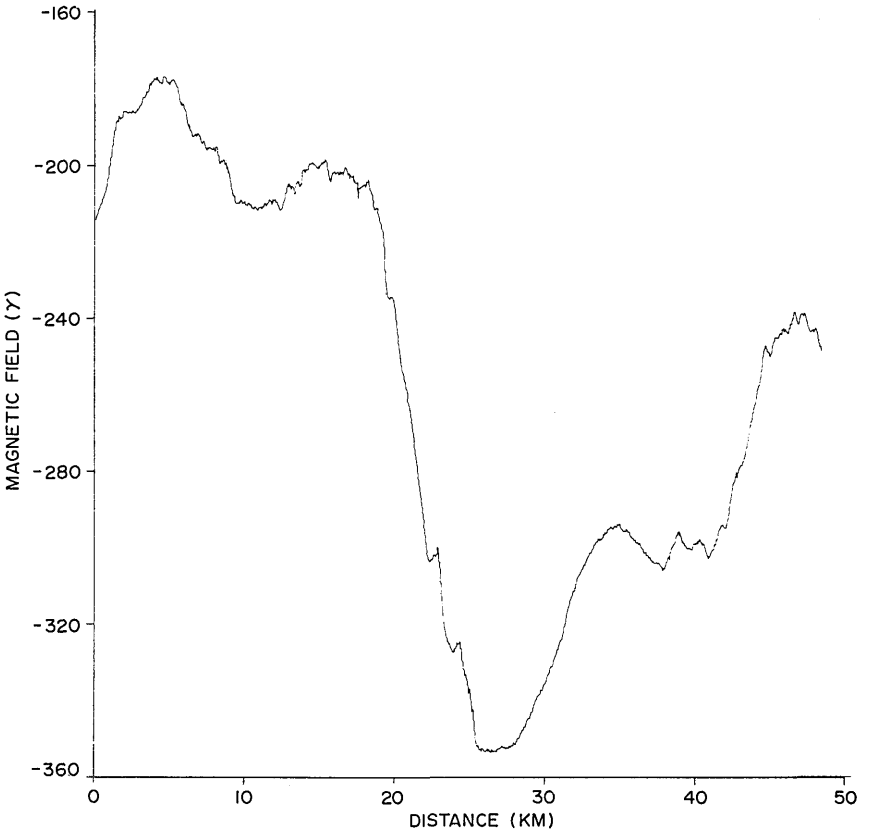

Fig. 12a — Residual field vs distance for Track 6

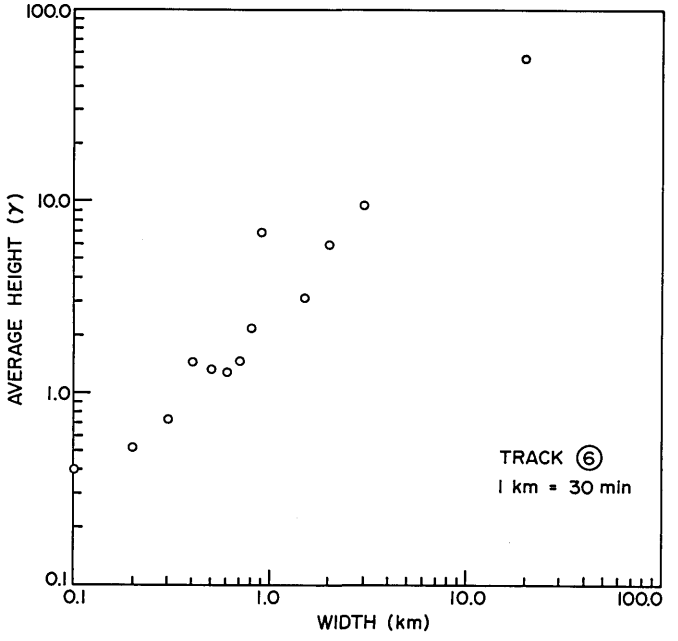

Fig. 12b — Spectrum of average peak heights vs corresponding wavelengths for Track 6

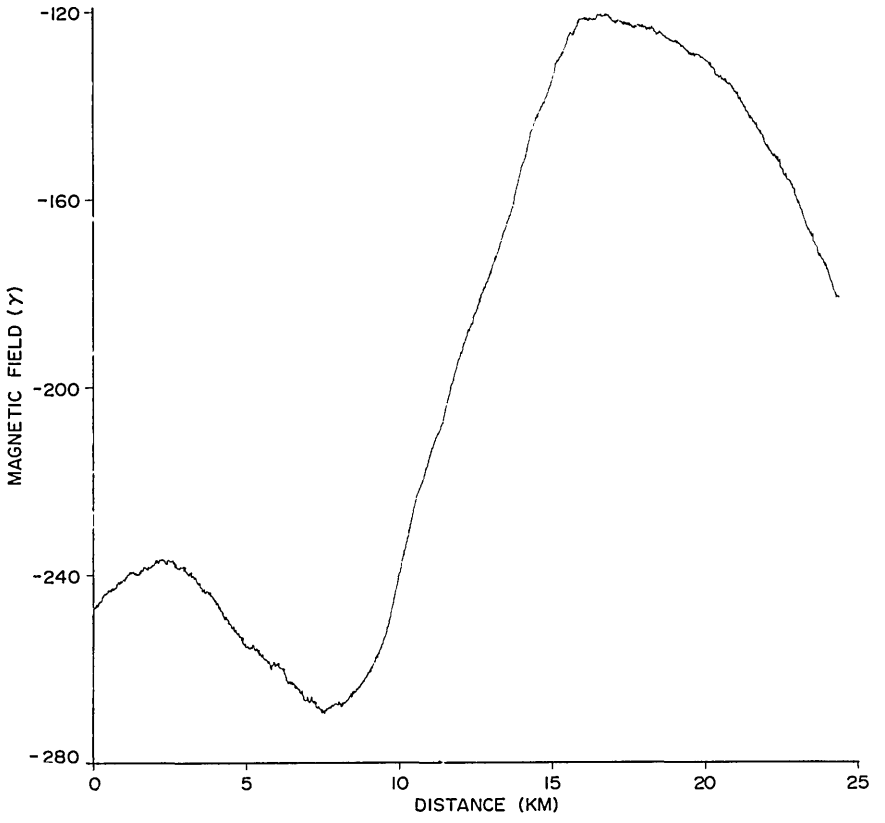

Fig. 13a — Residual field vs distance for Track 7

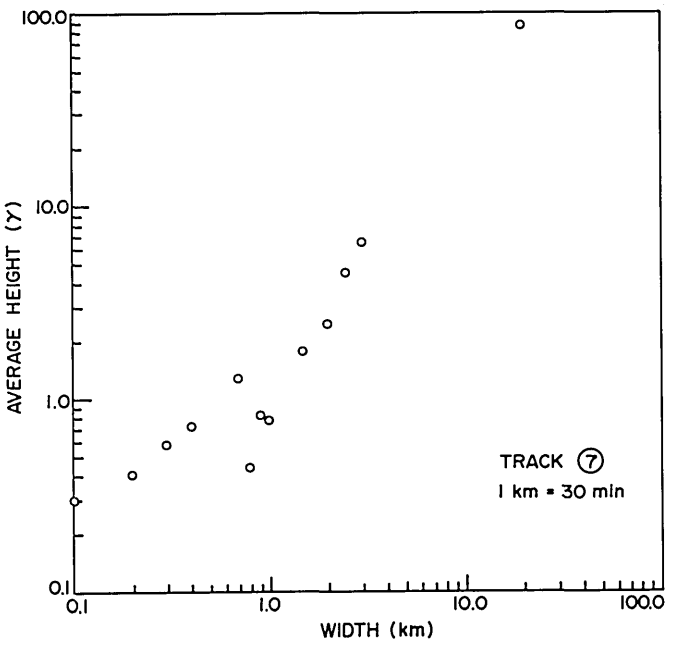

Fig. 13b — Spectrum of average peak heights vs corresponding wavelengths for Track 7

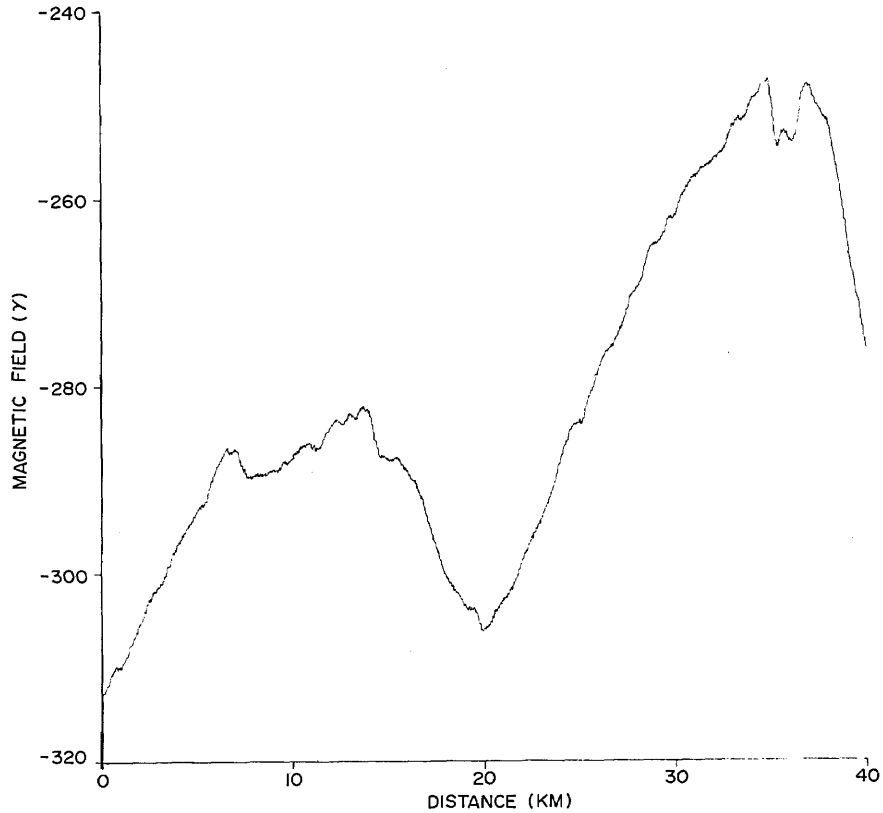

Fig. 14a — Residual field vs distance for Track 8

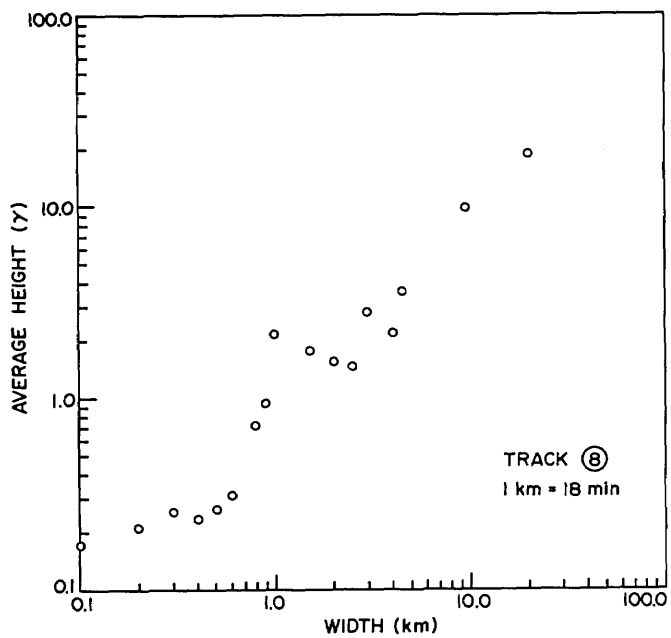

Fig. 14b — Spectrum of average peak heights vs corresponding wavelengths for Track 8

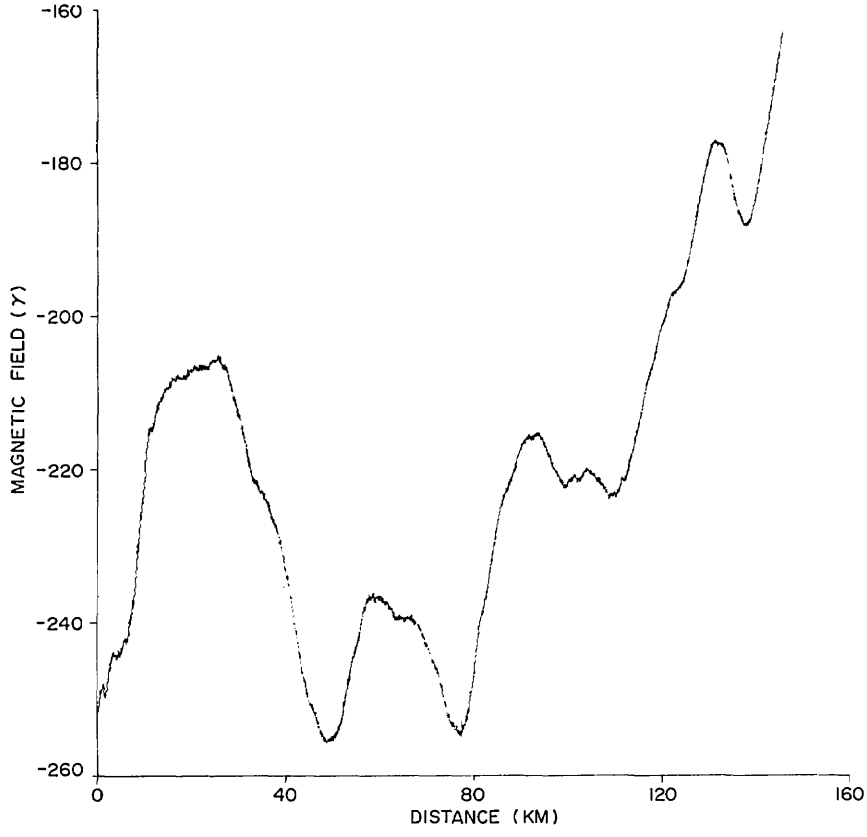

Fig. 15a — Residual field vs distance for track made in quiet zone

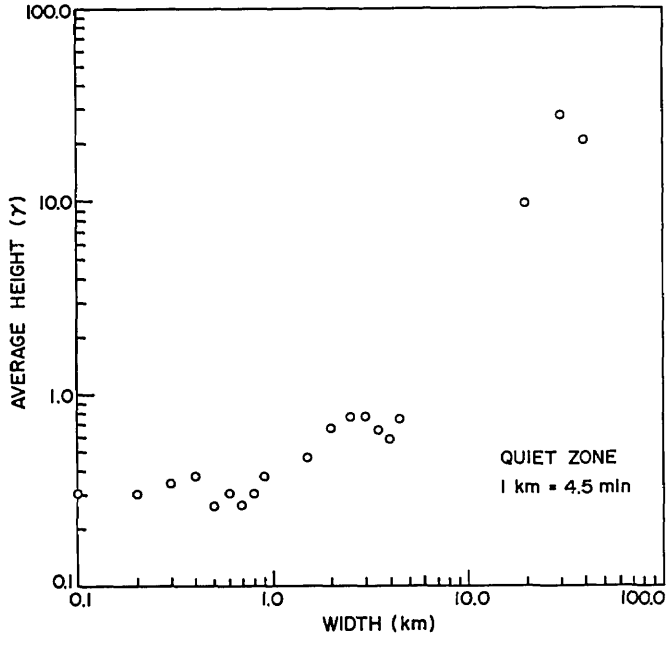

Fig. 15b — Spectrum of average peak heights vs corresponding wavelengths for quiet zone track

Despite the absence of short-wavelength geological features, the Bermuda area should be considered moderately noisy, magnetically. For comparison, we include in Figs. 15a and 15b a set of surface data taken on another trip in the quiet zone (36°N, 70°W). The day was magnetically quiet and the sea calm. The results show that the geological features present are lower in amplitude and longer in wavelength than those around Bermuda. The major source of noise was probably due to motions of the transducer at the towing speed of the ship, 8 knots.

All of the data taken on this cruise are recorded on magnetic tape and are readily available for further calculations.

ACKNOWLEDGMENTS

We acknowledge the vital assistance of Dr. P. T. Taylor of Naval Oceanographic Office who accompanied us on the first half of the trip and who provided us with a new reel of cable for the deep magnetometer after we found that the one we were using was unsuitable. We further acknowledge the assistance of Mr. J. L. Gregson III of the Ocean Sciences Division and Mr. Ray Phalen and Mr. Ralph Gallatin of the Ship Facility Group (Code 8004), who were also members of the scientific party. In addition, the Master, officers, and crew of the USNS MIZAR were unfailingly helpful and cooperative.

The computer program for calculation of the IGRF was kindly made available to us by Mr. L. P. LaLumiere of the Acoustics Division, NRL.

Appendix A

TWO TECHNIQUES FOR STUDY OF THE SHORT-WAVELENGTH FEATURES OF THE MAGNETIC FIELD

J. M. Bergin

BACKGROUND

One objective of our program is to study those variations of the total surface magnetic field which occur over a distance of a few kilometers. These variations will generally be small in amplitude, and it is necessary to separate them from the much larger variations that occur over longer distance scales. We can accomplish this separation by filtering the data. In this section we compare two techniques of filtering to determine their relative merits. Before proceeding with the discussion of filters we will first comment on the form of our data.

The measurements consist of values for the total surface and deep magnetic fields at equally spaced time intervals along the ship's track, position fixes at various time intervals for the ship, and a few auxiliary quantities which will not play any role in the present discussion. Our measurements of the surface field are made approximately 200 m beneath the ocean surface, while the deep field is measured at a depth of a few kilometers. We deal with the surface field alone in this section, although the general methods are equally applicable to any field measurements. Since we want to study the wavelength content of the magnetic field, the primary observations of field vs time are converted to field vs distance along the ship's track through use of the position data, which is known as a function of time.

The resulting data of magnetic field vs distance may contain errors associated with observational errors in the position data. In addition, geomagnetic noise and field variations caused by oceanic wave motion introduce errors into the field data. The major components of geomagnetic noise occur in the distance data at long wavelengths outside the range of interest, but there will undoubtedly be some contribution to the short wavelengths. Magnetic variations caused by oceanic wave motion are limited to the vicinity of the ocean surface and generally will amount to at most a few gammas. We do not discuss these sources of noise any further in this section, but rather move on to a description of methods for determining the wavelength content of the data. To study the short-wavelength behavior of the magnetic field, we want a numerical technique that operates on the original field-vs-distance data and yields a set of "filtered" values of field vs distance in which variations with wavelengths outside some specified range of interest have been suppressed.

There are essentially two approaches which can achieve such filtering of the original data. We designate these two approaches as local filtering and global filtering. In the local method of filtering, the filtered value for a particular position along the track is obtained by averaging a small portion of the original data located in the vicinity of the given position. This local method would seem to correspond to the electrical filtering of

data by airborne sensors whose purpose is to locate magnetic anomalies. Global filtering, on the other hand, utilizes the entire set of data values for generating each value of the filtered series.

LOCAL FILTERING

We now present the basic mathematical procedure for local filtering. Holloway (A1) gives a detailed treatment of the procedure. Suppose that our magnetic field data consist of N values $M(j)$, $j = 0,1,\ldots, N\text{-}1$, determined at equally spaced distance intervals $\Delta\chi$. Then the filtered data $\overline{M}(j)$ are given by the sum

$$\overline{M}(j) = \sum_{k=-\ell}^{\ell} w(k)M(j+k) \qquad j = \ell,\ell+1,\ldots,N-\ell-1 \tag{A1}$$

in which the weights w(k) are defined in terms of the continuous filter function $W(x)$ by $w(k) = \Delta\chi\ W(k\Delta\chi)$. The frequency response function defined by

$$R(f) = \int_{-\ell\Delta x}^{\ell\Delta x} W(x)\ \exp\ (2\pi i f x)\ dx \tag{A2}$$

provides information about the effect of the filter on a component of frequency f occurring in the original data $M(j)$. In particular if the original data have a component of frequency f and amplitude A, then the amplitude of this component in the filtered data is $|R|A$. Thus, those frequencies for which the magnitude of the response function $R(f)$ is zero or extremely small are effectively absent from the filtered data.

The technique of local filtering we shall employ is to process the original data with a low-pass filter with response function R_1 to remove very high frequencies and then to process the filtered data with a high-pass filter with response function R_2 to remove very low frequencies. The resultant effect of these two operations is to subject the original data to a band pass filter whose frequency response function is given by the product R_1R_2.

The filter functions have the form

$$W(x) = \frac{1}{2\ell\Delta x}\left(1 + \cos\frac{\pi x}{\ell\Delta x}\right) - \ell\Delta x \leqslant x \leqslant \ell\Delta x\,. \tag{A3}$$

Application of Eq. (A2) leads to the response function

$$R(f) = \frac{\sin\ 2\pi\ell f}{2\pi\ell f}\left(\frac{1}{1-(2\ell f)^2}\right), \tag{A4}$$

in which the frequency appears in cycles per data interval. This response function is plotted in Fig. A1. Since the response function effectively vanishes at high frequencies, we see that Eq. (A3) represents a low-pass filter. The parameter ℓ, which is related to the

number of data values used to construct a filtered value, determines the range of frequencies passed by the filter. In an actual calculation a value for ℓ must be found to achieve the desired attenuation of the high-frequency components.

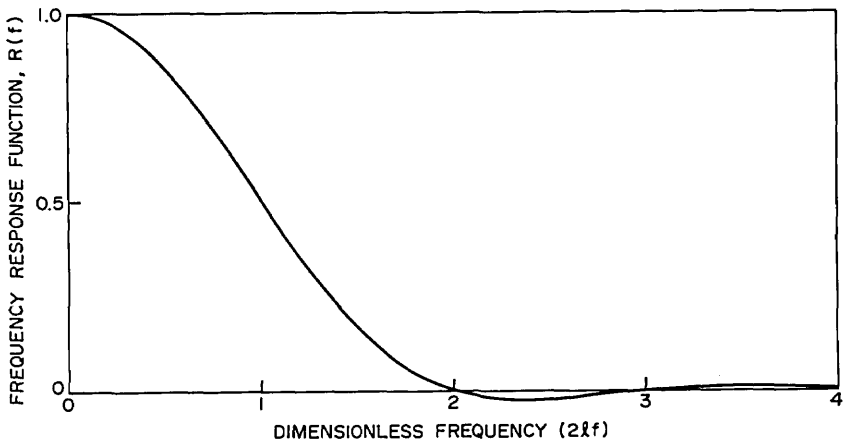

Fig. A1 — Frequency response function for a low-pass filter. The frequency f is in cycles data interval. The parameter ℓ is an integer related to the number of data points used to form a filtered value; ℓ also determines the width of the filter.

The high-pass filter we employ has a frequency response function equal to 1–R, where R has the general form given by Eq. (A4). Different values of the parameter ℓ are used for the low-pass and high-pass filters. The problem of selecting an appropriate value for the parameter ℓ is more critical for the high-pass filter than it is for the low-pass filter because the amplitudes of the low-frequency components we want to remove are usually quite large compared to the amplitudes of those components we want to retain. Thus, we require a rapid decrease of the frequency response function at low frequencies.

In Fig. A2 we show the frequency response function for a bandpass filter constructed from filter functions of the form given in Eq. (A3). We shall apply this bandpass filter to data for which one data interval = 0.033 km. From the figure we then determine that the responses function equals 0.5 at wavelengths approximately equal to 0.33 and 5.3 km. Wavelengths outside this band are attenuated in varying degrees as indicated by the behavior of the response function; thus we can regard the above wavelengths as approximately defining the passband of the filter.

We shall apply local filtering to the data plotted in Fig. A3a. This figure shows values of the total magnetic field as a function of distance along the track plotted in Fig. A3b. There are 2160 values of the magnetic field at a spacing of 0.033 km. The change in course shown in the bottom right-hand corner of Fig. A3b produced the large oscillation in field values located just before the 20-km mark in Fig. A3a. This oscillation arises because the field variation with distance along a track is highly dependent on the orientation of the track relative to contour lines of the total magnetic total field. Although this large amplitude oscillation is artificial, it does simulate the effect a seamount might have, and we shall find it instructive to examine what effect the two filtering methods have on this large amplitude oscillation.

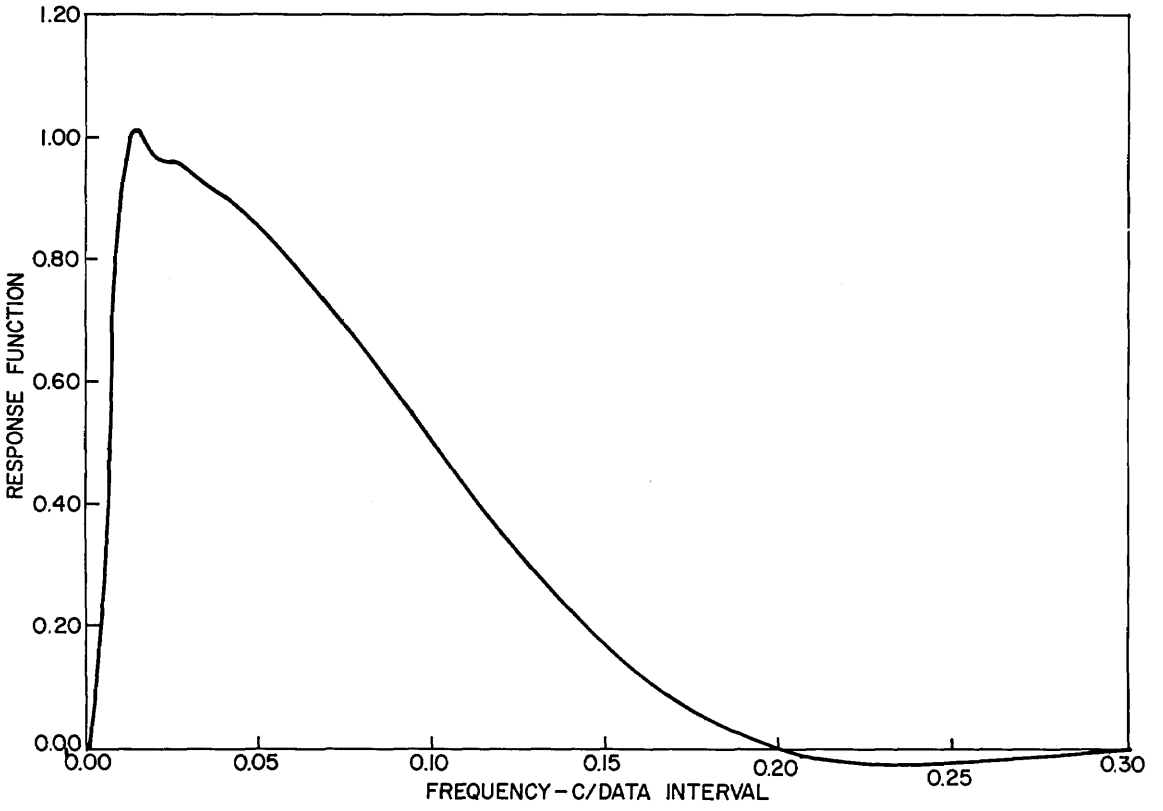

Fig. A2 — Frequency response function for a band pass filter. For the data to which this filter is applied, 1 data interval = 0.033 km. The wavelength band lies in the approximate range of 0.5-3 km.

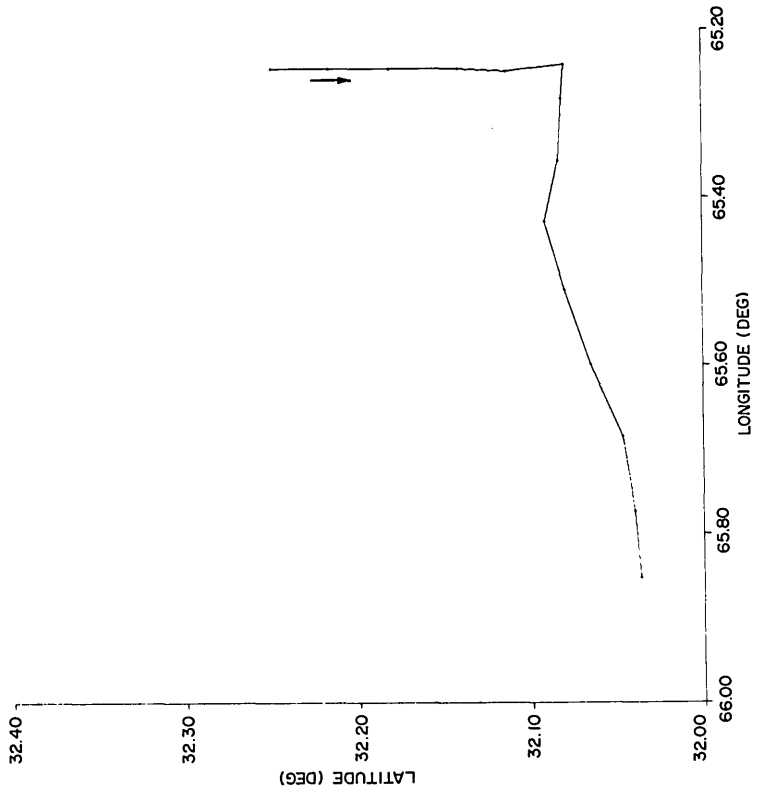

Fig. A3b — Track of the ship along which the data in Fig. A3a was measured. The arrow indicates the direction of travel. Latitude is north latitude, longitude is west longitude. Position fixes are indicated by solid points and are joined by straight lines.

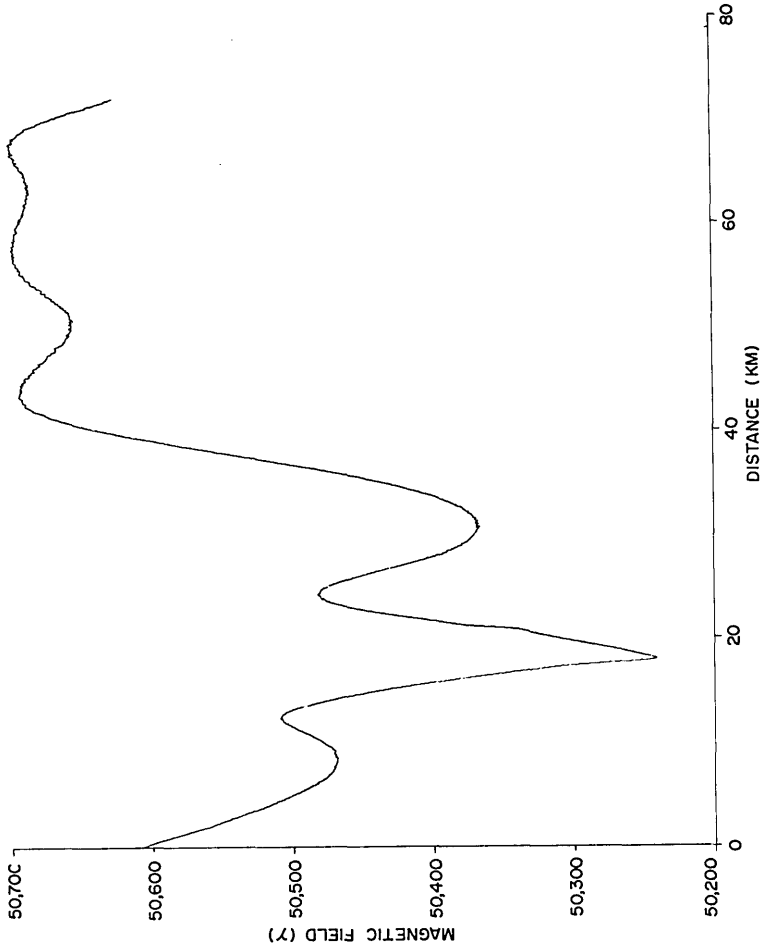

Fig. A3a — Total surface magnetic field as a function of distance. The plot consists of 2160 readings, which are connected by straight lines, at a spacing of 0.033 km.

When the bandpass filter of Fig. A2 is applied to the data of Fig. A3a we obtain the results shown in Fig. A4. It is clear from the behavior of the filtered data in Fig. 4 that residual oscillations of large wavelength, greater than 10 km for example, remain in the filtered data. These residual oscillations have amplitudes much larger than the amplitudes of components lying within the passband of the filter and, consequently, tend to obscure the latter components. The fact that local filtering of the data fails to completely remove components outside the passband of the filter represents a further disadvantage of this method of filtering.

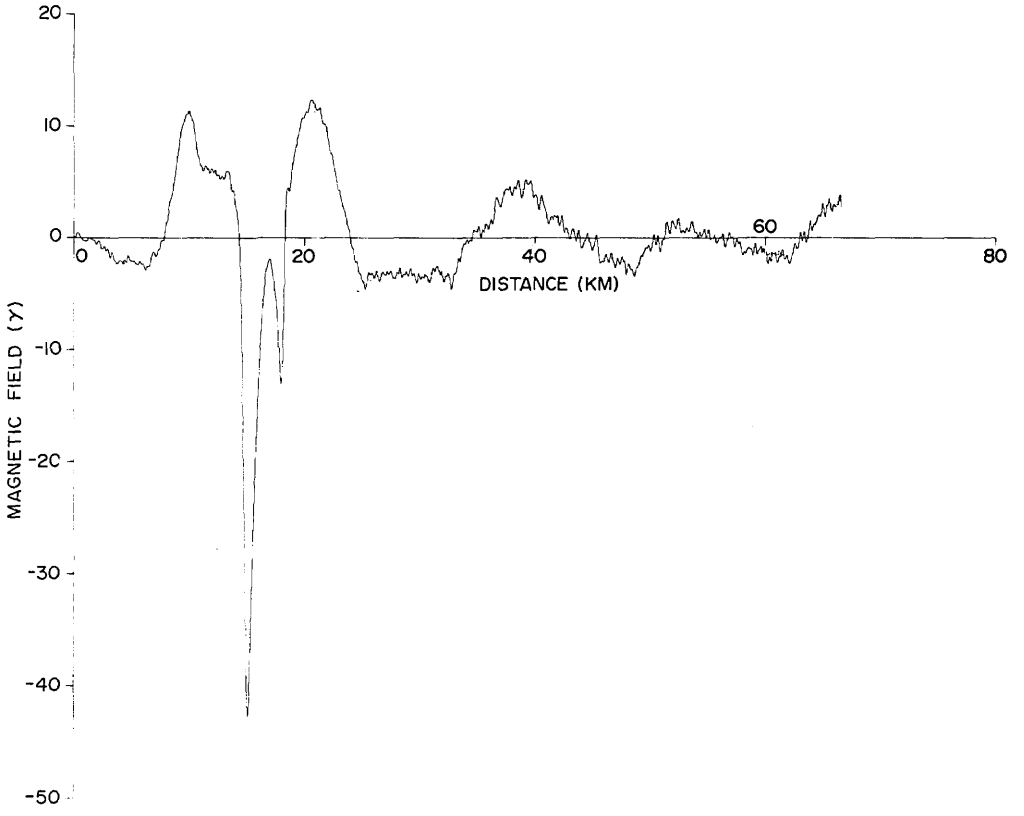

Fig. A4 — Result of applying the band-pass filter of Fig. A2 to the data shown in Fig. A3a.

The largest peak in the filtered data occurs just before the 20-km mark and is associated with the course change. We note that this peak has a wavelength of approximately 3 km while the original anomaly produced by the course change has a wavelength of about 10 km. This demonstrates that large amplitude variations of long wavelength can produce short-wavelength oscillations of significant amplitude in the filtered output. We shall find later that this statement applies to the global method of filtering as well.

It is of some interest to determine what effect the bandpass filter has on a specific short-wavelength feature present in the data. To accomplish this we artificially introduced into the original data of Fig. A3a an anomaly consisting of one oscillation of a sine wave having an amplitude of 5γ and a wavelength equal to 1 km. The modified data are shown in Fig. A5 with the artificial anomaly located at a distance of 47.5 km. When we apply the bandpass filter to the data of Fig. A5 we obtain the result shown in Fig. A6. The artificial anomaly is much more distinct in the filtered data. We note that its amplitude and wavelength are essentially unchanged by the filter. The anomaly no longer occurs at 47.5 km because of the nature of the filtering operation; in effect, the curve in Fig. A6 should be translated to the right by about 2.8 km to have distances correspond with those appearing in Fig. A5.

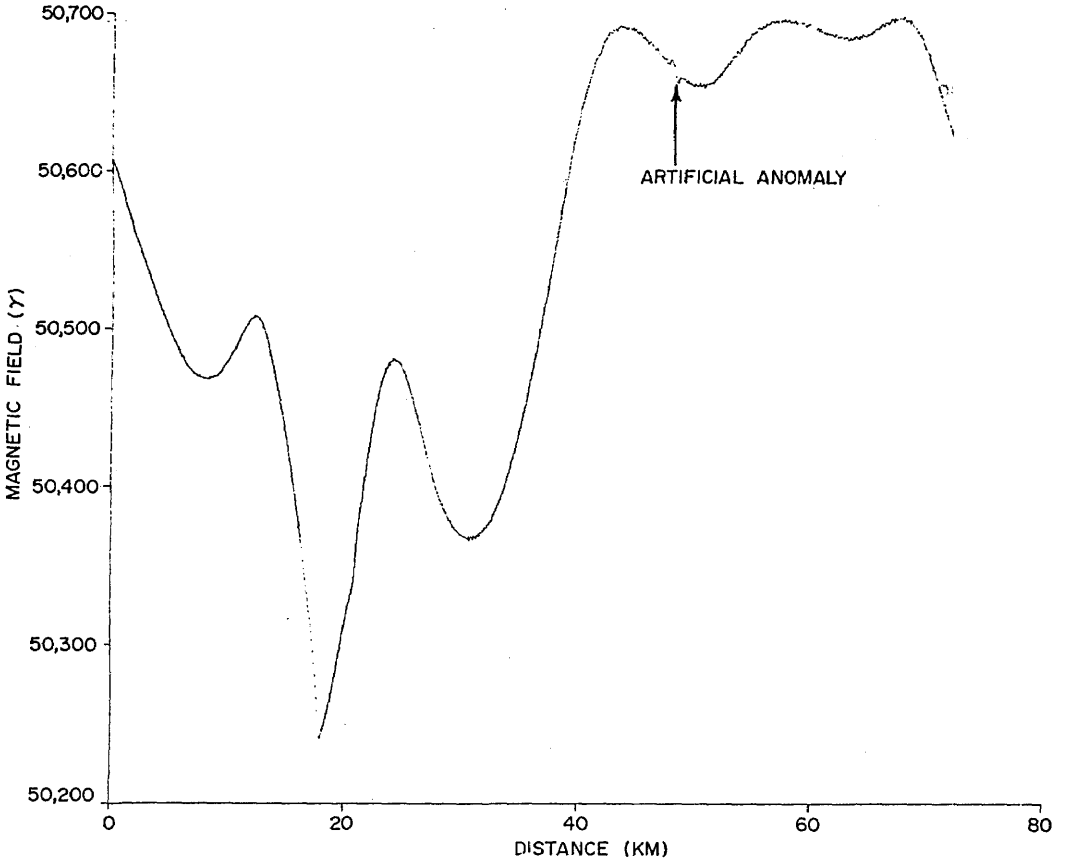

Fig. A5 — Data of Fig. A3a modified by the inclusion of an artificial anomaly. The anomaly consists of one wavelength of a sine wave having an amplitude of 5γ and a wavelength of 1 km.

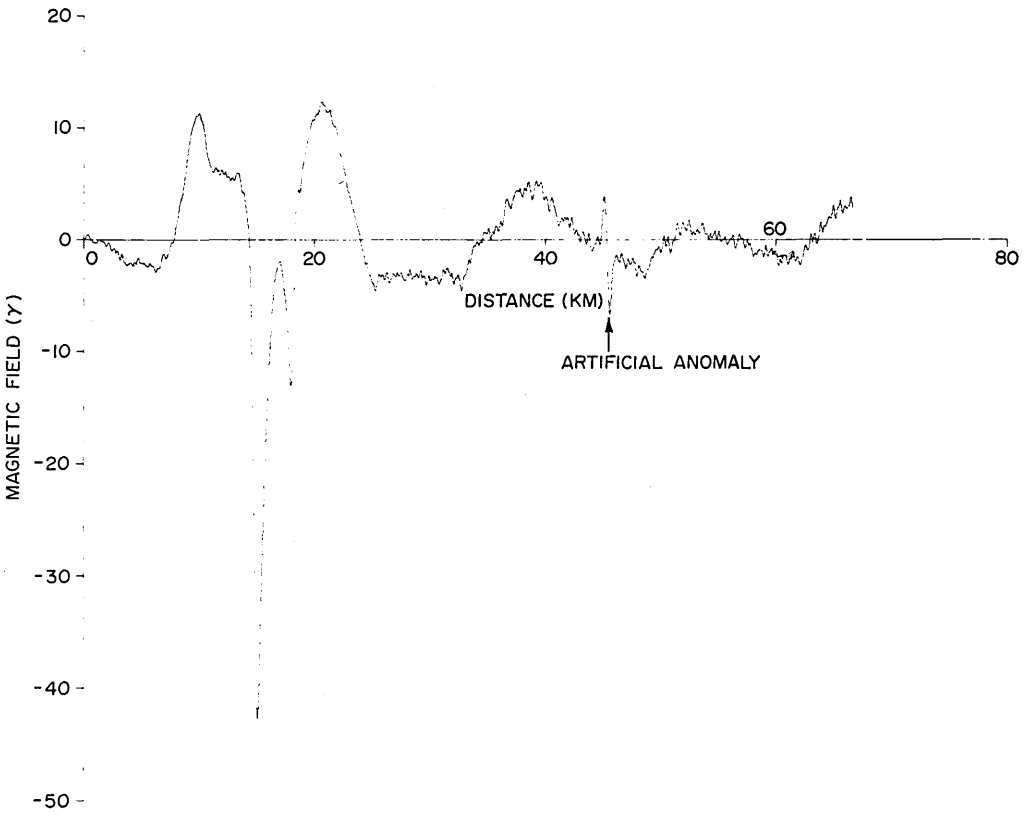

Fig. A6 — Result when the data of Fig. A5 is passed through the band pass filter shown in Fig. A2.

GLOBAL FILTERING

We now present the essentials of a method of global filtering based on the discrete Fourier transform, which we shall abbreviate DFT. The DFT method will be seen to represent an ideal band pass filter in the sense that components with frequencies outside the band of interest can be entirely removed from the data. We first give the basic relationships of the DFT that will be needed in our discussion of global filtering.

Let $M(j)$, j =0, 1,..., N-1 again represent N values of the magnetic field measured along a track in such a way that the data values are at equally spaced distance intervals Δx. We shall assume, for convenience, that the number N of data values is even. The first step in the method involves the calculation of the discrete Fourier transform of $M(j)$. The DFT is defined by

$$A(n) = \frac{1}{N} \sum_{j=0}^{N-1} M(j) \exp(-2\pi i n j/N) \tag{A5}$$

in which n = 0, 1, ..., N-1 and i denotes $\sqrt{-1}$. The inverse of the DFT in Eq. (A5) is given by

$$M(j) = \sum_{N=0}^{N-1} A(n) \exp(2\pi i n j/N) \tag{A6}$$

with j = 0, 1, ..., N-1. It is advantageous to regard the expressions in Eqs. (A5) and (A6) as defined for all integer values of n and j, respectively. Both expressions then become periodic with period N. The DFT and its inverse are easily calculated on a computer with the use of the fast Fourier algorithm developed by Cooley and Tukey (A2). For a discussion of the discrete Fourier transform and the computational algorithm we refer the reader to Cooley, Lewis, and Welch (A3).

Our data always consist of real values for $M(j)$, and this implies that the $A(n)$ appearing above must satisfy

$$A\left(\frac{N}{2} + n\right) = A^*\left(\frac{N}{2} - n\right) \tag{A7}$$

for n = 0, 1, ..., $N/2$. The asterisk designates complex conjugate. Equation (A7) allows us to write Eq. (A6) in the form

$$M(j) = A(o) + \sum_{N=1}^{N/2}{}'\left(2 \text{ Re } A(n) \cos\frac{2\pi n j}{N} - 2 \text{ Im } A(n) \sin\frac{2\pi n j}{N}\right), \tag{A8}$$

where the prime on the sum indicates that the term for $n = N/2$ must be halved. The real and imaginary parts of $A(n)$ are designated by Re $A(n)$ and Im $A(n)$. Equation (A8) represents the discrete data $M(j)$ as a sum of periodic terms, much as the Fourier series development represents continuous data on a finite interval. The following table indicates the frequency, wavelength, and amplitude associated with each term of the representation in Eq. (A8).

Table A1
Frequency, Wavelength, and Amplitude of Each Fourier Component

Value of n	Dimensionless frequency (cyc/data interval)	Frequency†	Wavelength	Amplitude of component
0	0	0	∞	$\lvert A(o)\rvert$
$0 < n < \frac{N}{2}$	$\frac{N}{N}$	$\frac{N}{N\Delta x}$	$\frac{N\Delta x}{M}$	$2\lvert A(n)\rvert$
$\frac{N}{2}$	$\frac{1}{2}$	$\frac{1}{2\Delta x}$	$2\Delta\chi$	$\lvert A(N/2)\rvert$

†Δx = distance increment between field readings.

The highest frequency present, $1/(2\Delta x)$, is the Nyquist cutoff frequency and is caused by sampling at finite intervals. A plot of the amplitudes with respect to wavelength would provide the amplitude spectrum of the data $M(j)$. Similarly, other types of spectral plots can be constructed from the information in the table.

The procedure in global filtering is as follows. First, we select a sequence of values $M(j)$ of the magnetic field whose wavelength structure we wish to examine. Let us assume that we are interested in the wavelength range λ_1 to λ_2, (where $\lambda_1 < \lambda_2$). We then calculate the DFT of the data $M(j)$ so that we now have available the coefficients $A(n)$. Each $A(n)$ is associated with a definite wavelength as indicated in the table above. For each $A(n)$ we determine if its associated wavelength $\lambda(n)$ lies within the wavelength band λ_1 to λ_2 of interest. If $\lambda(n)$ does not lie in the band we set $A(n) = 0$. Those $A(n)$ whose wavelengths are in the band λ_1 to λ_2 are left unchanged. Once this procedure has been completed, we calculate the expression in Eq. (A8) (or equivalently Eq. (A6)) using the new set of coefficients $A(n)$. This provides us with our filtered data $\overline{M}(j)$. Since we have set the amplitude of each component with a wavelength outside the band λ_1 to λ_2 equal to zero, it is clear that our filtered data $\overline{M}(j)$ contain only those wavelengths that lie in the band of interest.

The reason for calling this technique global filtering stems from the fact that each of the coefficients $A(n)$ depends on the entire sequence of data values $M(j)$, as is clear from the form of the expression in Eq. (A5). Thus, in order to calculate each value of the filtered data $\overline{M}(j)$ we must use the entire sequence of original data $M(j)$.

Figure A7 shows a plot of the amplitude spectrum of the data of Fig. A3a. The spectrum was calculated using the DFT described above. We should point out that for N data values, N even, the DFT generates $N/2$ spectrum values. We joined the spectrum values by straight lines in the figure to provide a more definite visualization of the nature of the spectrum.

In Fig. A8 we show the data of Fig. A3a after it has been filtered by the global method with a wavelength band of 0.5 to 3 km. Figure A8 is to be compared with Fig. A4, which represents local filtering of the same original data for approximately the same wavelength band. Clearly the global or DFT method removes the longer wavelengths outside the band, whereas local filtering leaves residual variations in these longer wavelengths.

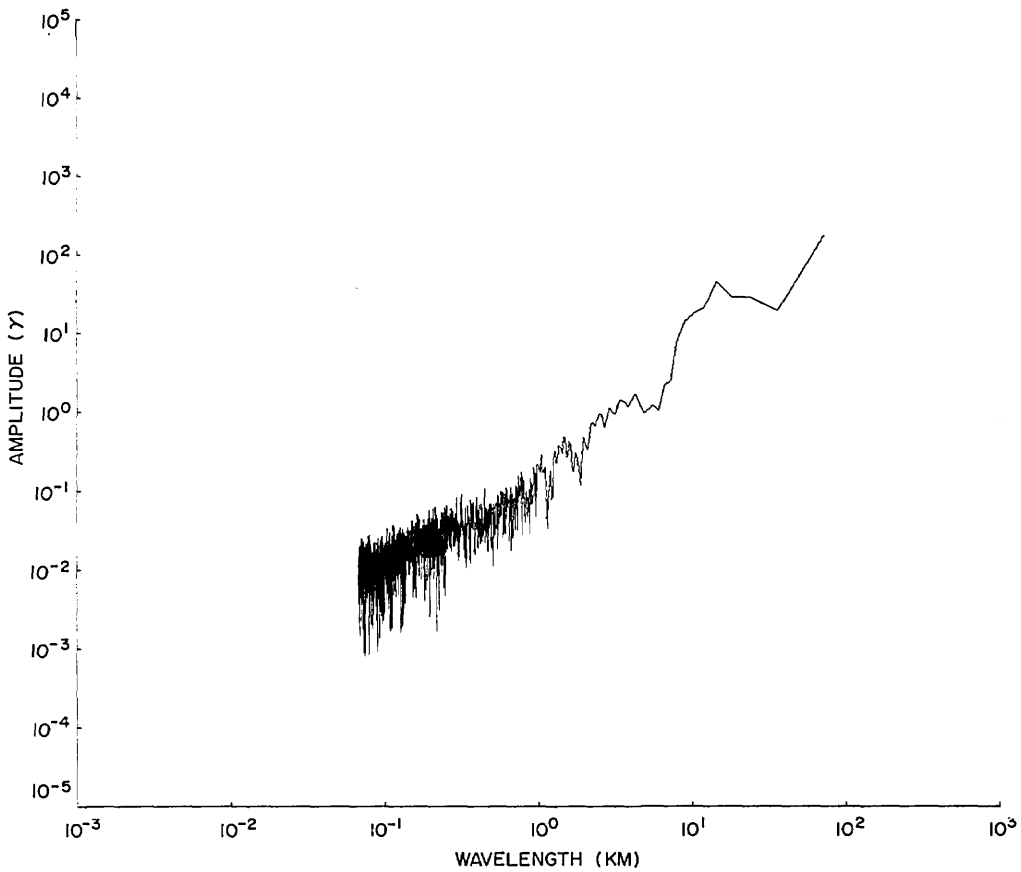

Fig. A7 — Amplitude spectrum of the original data shown in Fig. A3a. Spectrum values are joined by straight lines to emphasize the nature of the spectrum.

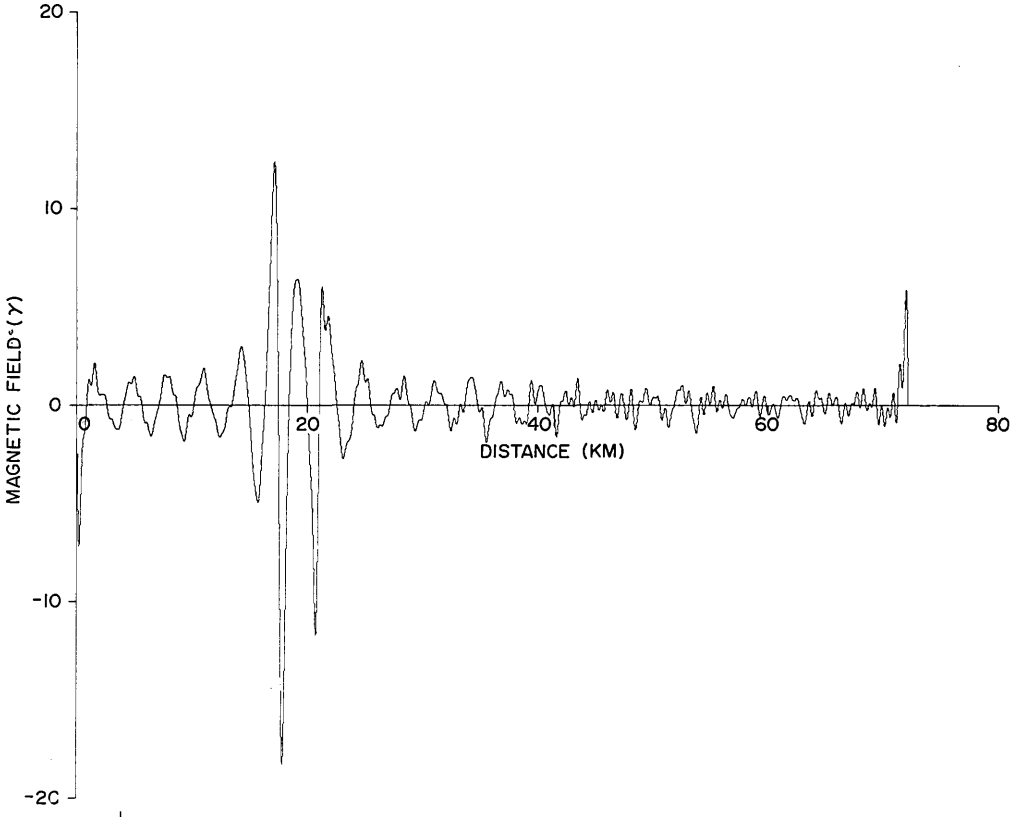

Fig. A8 — Result of applying the global method of filtering to the original data shown in Fig. A3a. The wavelength band passed by the filter extends from 0.5-3 km. The peaks at the beginning and end of the record are artifices of the mathematical method.

The major feature at about 20 km in Fig. A8 arises from the change in course shown in Fig. A3b. We again find that this feature with a wavelength of approximately 10 km contributes to the short-wavelength structure of the filtered data.

We should point out that the peaks at the beginning and end of the plot in Fig. A8 are due to the mathematical method of the DFT which assumes that the given data represent a periodic function of distance. This usually means that discontinuities in the behavior of the function occur at the beginning and end of the data record. These discontinuities often lead to the presence of large-amplitude, short-wavelength oscillations of the type we see in Fig. A8 at the beginning and end of the record. Thus, we must regard such behavior as an artifice introduced by the mathematical method rather than as a consequence of the true behavior of the magnetic field. As a matter of routine, in processing the field data, we subtract from the original data the International Geomagnetic Reference Field and a linear field to make the final data value equal the initial data value. The subtracted fields are of no interest for short-wavelength structure, and the removal of the linear field tends to reduce the end effects.

Figure A9 shows the result of filtering the data given in Fig. A5 by the global method, with the wavelength band from 0.5 to 3 km. It will be recalled that Fig. A5 is a plot of the original data modified by the inclusion of an artificial anomaly (one oscillation of a sine wave with a 5γ amplitude and a 1-km wavelength) at a distance of 47.5 km. Figure A9 is to be compared with Fig. A8, which shows the result of filtering the original data when the artificial anomaly is absent. We see that the amplitude and wavelength of the anomaly are essentially unaffected by the filtering operation and that good resolution of the anomaly is achieved. We can also compare Fig. A9 with Fig. A6, which shows the result of filtering the same data by the method of local filtering. Resolution of the anomaly is approximately the same for both methods as far as the present data are concerned.

SUMMARY

These results indicate that the global method of filtering based on the discrete Fourier transform has the following definite advantages over the local method of filtering.

1. The global method removes those components whose wavelengths are outside the band of interest and retains the correct amplitudes of the remaining components. On the other hand, the local method of filtering does not entirely remove those components not of interest and, in general, alters the amplitudes of all components.

2. Programming the global method for a computer is relatively simple, since subroutines are available for the rapid calculation of the discrete Fourier transform. To achieve good results with the local method it is necessary to have detailed information about the data so that values for certain parameters of the band pass filter can be properly selected. The selection of these values makes the local method somewhat difficult to apply.

3. In the global method the results of the calculation of the discrete Fourier transform can be used to compute power spectra, amplitude spectra, or other related quantities of possible interest.

We therefore selected the global method of filtering as the appropriate method to employ for the study of short-wavelength structure of the magnetic field.

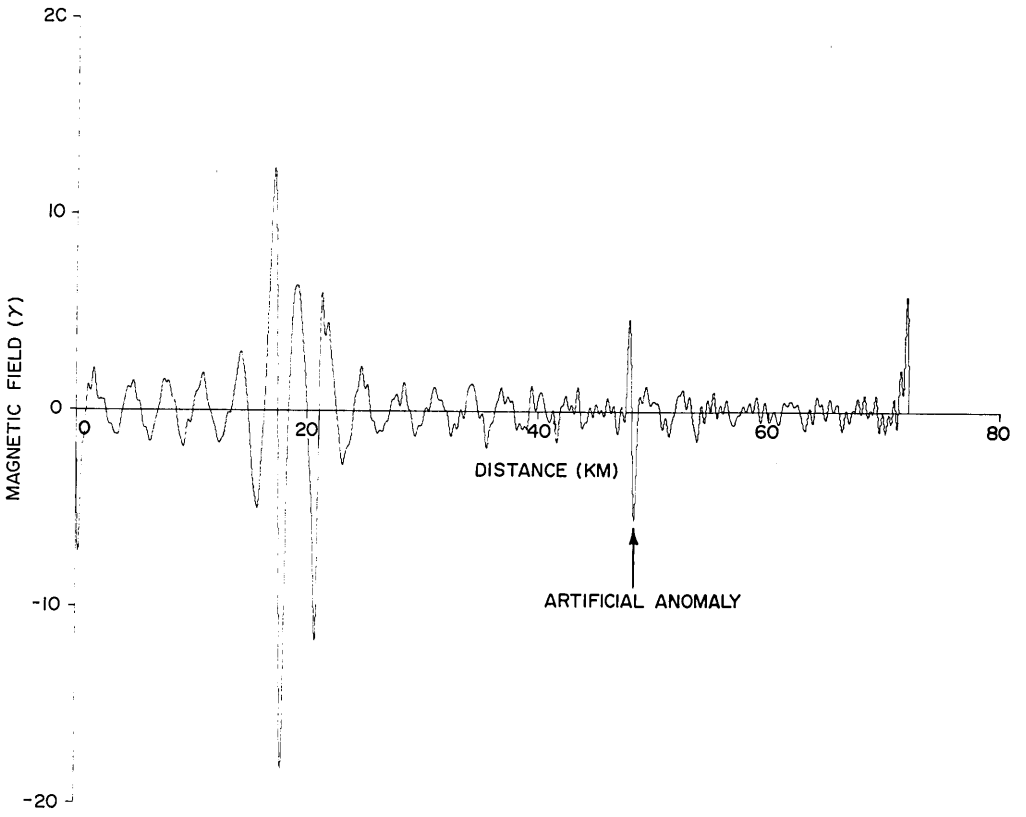

Fig. A9 — Result of applying the global method of filtering to the data of Fig. A5, which contains an artificial anomaly. The wavelength band passed by the filter extends from 0.5-3 km.

REFERENCES

A1. J. L. Holloway, Jr., "Smoothing and Filtering of Time Series and Space Fields," in *Advances in Geophysics*, Vol. 4, (edited by H. E. Landsberg and J. van Mieghem, eds.), Academic Press, Inc., New York, 1958.

A2. J. W. Cooley and J. W. Tukey, "An Algorithm for the Machine Calculation of Complex Fourier Series," Math. Comp. 19: 297-301 (1965).

A3. J. W. Cooley, P. A. W. Lewis, and P. D. Welch, "The Finite Fourier Transform," IEEE Trans. Audio Electroacoust. AU-17: 77-85 (1969).

*U.S. GOVERNMENT PRINTING OFFICE:1974 542-170/231 1-3